BL4B
Study of Magnetic Anisotropy in NO/Ni/Cu(001) Using X-Ray Magnetic Circular Dichroism

T. Nakagawa, Y. Takagi, I. Yamamoto and T. Yokoyama

Department of Electronic Structure, Institute for Molecular Science, Okazaki 444-8585, Japan

Magnetic anisotropy in a magnetic thin film is sensitive to its surface modification since the contribution of the surface to the entire film is significant and the surface atoms may exhibit non-collinear anisotropy due to their lower symmetry. It is known that the orbital moment, which is usually large at the surface and interface, is an origin of the magnetic anisotropy. To support this concept, the quantitative relationship between the orbital moment and the magnetic anisotropy needs to be examined. For this aim, X-ray magnetic circular dichroism (XMCD) under a strong magnetic field enough to saturate the magnetization is an ideal method.

XMCD experiments were carried out at BL4B, which delivers circular polarized light (circular polarization = 0.67). The end station was an ultra high vacuum chamber equipped with a superconductive magnet (7 T) and a low temperature insertion of 5 K. [1] 4 ML Ni films grown on a Cu(001) sample were used, which had magnetic easy axis within the surface, and NO adsorption did not change its easy axis. Adsorption of NO was done at 5 K, and the coverage of NO was estimated to be 0.5 ML as judged from XAS spectra.

Figure 1 shows XMCD spectra for grazing and normal incidences. From the XMCD sum rule, spin magnetic moment (m_s) and orbital magnetic moments for the in-plane ($m_{orb}^{//}$) and out-of-plane ($m_{orb}^{\perp}$) components are separately evaluated. The m_{orb} components are larger for the in-plane direction before and after NO adsorption, which is in agreement with the direction of the magnetization easy axis. Upon the NO adsorption the difference in m_{orb} between the out-of-plane and in-plane directions becomes smaller, suggesting that NO adsorption makes the in-plane anisotropy weaker.

Figure 2 shows magnetization hysteresis curves with the magnetic field normal to the surface, which were taken on the same sample as that for Fig. 1. The magnetization curves are results of Ni-L_3 intensity variation as a function of magnetic field. The anisotropy fields, H_a, are 2.1 and 1.0 T for clean and NO adsorbed surfaces respectively, resulting in anisotropy energies, K_u, of 5.1 x 10^5 and 1.9 x 10^5 J/m^3. The obtained anisotropy energies contain contributions from the shape anisotropy due to the dipole-dipole interaction and the electron orbital anisotropy (crystalline anisotropy). After the subtraction of the shape anisotropy (the clean and NO adsorbed surfaces are 1.6 x 10^5 for the clean surface and 1.2 x 10^5 J/m^3 for NO adsorbed surface), the

crystalline magnetic anisotropy energies are obtained as 3.5 x 10^5 and 0.7 x 10^5 J/m^3, respectively.

A theoretical model indicates that the difference of m_{orb} for in-plane and out-of-plane directions, Δm_{orb}, is simply proportional to the magnetic anisotropy energy. [2] From our result, the Δm_{orb} ratio between the clean and NO adsorbed surfaces is 0.013/0.002 ~ 6.5, which is in reasonably agreement with the crystalline anisotropy energies ratio (~5).
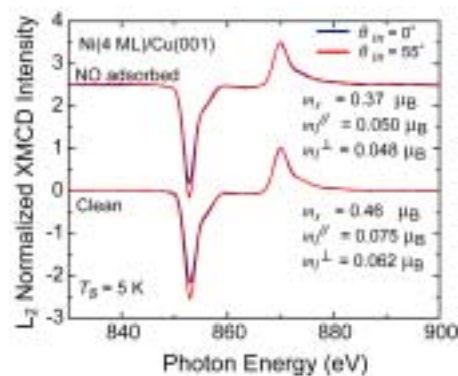
Fig. 1. XMCD spectra in Ni L edge for the clean and NO adsorbed surface. The calculated spin and orbital moments are indicated.
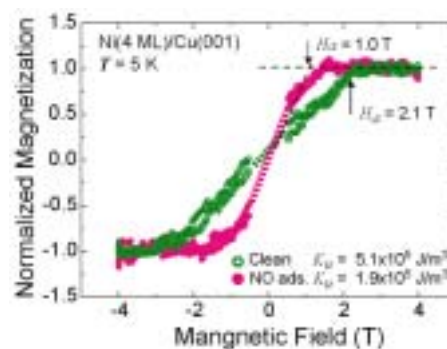
Fig. 2. Magnetization curves for clean Ni (4 ML)/Cu(001) and NO adsorbed one. Both the magnetic field and the photon incident direction are perpendicular to the surface. Anisotropy fields, H_a, are indicated.

[1] T. Nakagawa, Y. Takagi, Y. Matsumoto and T. Yokoyama, Jpn. J. Appl. Phys. **47** (2008) 2132.
[2] P. Bruno, Phys. Rev. B **39** (1989) 865.

Ⅲ-4. SURFACE AND THIN FILMS

Photoionization Threshold of Aromatic Molecules on the Surface of Ionic Liquid/Water Mixture

T. Ishioka, N. Inoue and A. Harata

Department of Molecular and Material Science, Kyushu University, Kasuga 816-8580, Japan

Photoionization threshold of aromatic molecules has been measured on the surface of the mixture of an ionic liquid and water. The threthold energy of pyrene was nearly unchanged with the content of water while the value of perylene was largely dependent on the ratio of water. This result suggests the solvation structure of pyrene at the surface is largely different from those of perylene.

Introduction

Ionic liquids have attracted much attention due to its unique characteristics such as low melting point, high conductivity, negligible vapor pressure, and designable solubility to other solvents. Their interfacial properties also attract large interest because interface structures play a crucial role in transport kinetics and they are related directly to the applications of ionic liquids such as solvent extraction and rechargeable batteries.

Interfacial characteristics of ionic liquids have been studied theoretically and experimentally. Surface tension measurements, X-ray techniques, neutron reflection, nonlinear optical methods, and molecular dynamic simulations have been used and their common conclusion on air/ionic liquid structure is that cations are present at the surface with long alkyl chains directed to the air. This conclusion implies surface molecules suffer different dielectric environment from those in bulk solutions.

The dielectric environment is directly related to the solvation conditions of solute molecules. However, it is difficult to know solvation conditions experimentally at the liquid surfaces. Photoionization is one of such methods to inform dielectric conditions at the surface because the threshold energy is lowered by the polarization energy of cations produced by photoionization.

In this report, photoionization thretholds of two aromatic molecules, pyrene and perylene, were measured at the surface of the mixture of ethylammonium nitrate and water. The water content was varied from 0-100% and the solvation characteristics were discussed.

Experimental

The monochromated synchrotron light (4-8 eV) was obtained from BL1B at the UVSOR facility and emitted from the chamber to the He-purged cell through an MgF_2 window. The emitted light was reflected on an Al mirror and vertically irradiated on the solution surface through a Cu-mesh electrode. The electrode was set at 5 mm high above the liquid surface and high voltage (400 V) was applied to the electrode so that emitted electrons were trapped. The photocurrent (~100 fA) was measured by a picoammeter and the incident photon intensity was monitored by measuring fluorescence intensity from sodium salicylate plate.

Solution samples were prepared by spreading dilute hexane solution of pyrene or perylene on the surface of the mixture of ethylammonium nitrate and water.
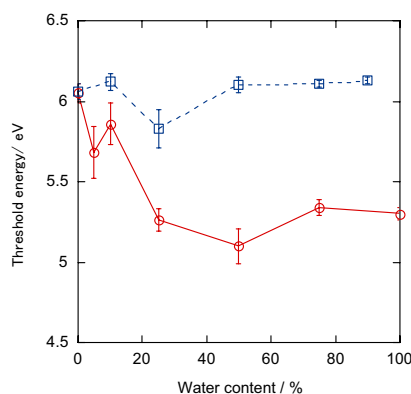
Fig. 1. Photoionization threshold energy of aromatic molecules on the surface of ethylammonium nitrate / water mixture. Solid line: perylene. Broken line: pyrene. The threshold value was derived from the mathematical fitting of $I= C(E-E_{th})^{2.5}$. I : photocurrent, C: constant, E: Photon energy.

Results and Discussion

Photoionization threshold energy (E_{th}) on the solution surface can be explained by

$$E_{th} = IP + P^+ \qquad (1)$$

where IP is ionization potential in vacuum and P^+ is the polarization energy. IPs of pyrene and perylene are 7.43 eV and 6.96 eV, respectively. From Fig. 1 measured photoionization threshold shows 0.9-1.8 eV lower value than each IP, indicating P^+ values. P^+ is the function of surrounding solvent properties such as dielectic constant and coordination numbers. In the case of pyrene, the threshold value is independent of water content. This result suggests dielectric condition of pyrene is not affected by bulk water content. While this, photoionization threshold of perylene decreases by increasing the water content showing large solvation energy by surrounding molecules. It is suspected that the average molecular distribution from the surface of perylene is deeper than pyrene.

Optical Properties of TiO_2 Thin Films Prepared by a Sol-Gel Method

T. Kawai[1], R. Sato[1] and K. Kifune[1,2]

[1]Department of Physical Science, Graduate School of Science, Osaka Prefecture University, Osaka 599-8531, Japan

[2]Faculty of Liberal Arts and Sciences, Osaka Prefecture University, Osaka 599-8531, Japan

Titanium dioxide (TiO_2) is one of technologically important materials from the view point of applications, such as pigments, photocatalyst, and dye sensitized solar cell [1]. Though a lot of studies on TiO_2 have been performed for structural and photocatalytic properties, the studies on optical properties of TiO_2 in the energy region above the band edge, especially up to the vacuum ultraviolet (VUV) energy region, have been considerably limited. In this study, we prepared TiO_2 thin films on the quartz substrate by using a conventional sol-gel method and performed the optical measurements up to the VUV energy region at the BL-1B line of UVSOR.

Figure 1 shows the absorption spectrum of the TiO_2 thin film. The absorption spectrum exhibits the rise at 3.32 eV, whose value is almost equal to the band gap of anatase TiO_2 crystals [2, 3]. Reflecting the ultra thinness of the sample, the several absorption peaks and shoulders can be seen in the energy region above the absorption band edge. We decompose the absorption spectrum of the TiO_2 thin film into the several Gaussian shape bands. The Gaussian shape bands obtained by decomposing the absorption spectrum are represented by blue curves in Fig. 1. These results are consistent with the absorption spectra calculated from the reflection spectra by Kramers-Kronig (K-K) transformations [2]. The experimental and theoretical studies for anatase TiO_2 crystals present that the highest valence band is composed of oxygen 2p states and the conduction bands below about 8 eV consist mainly of titanium 3d states [2, 3]. Therefore, these absorption bands are attributed to the transitions from oxygen 2p to titanium 3d states.

Figure 2 shows the luminescence and excitation spectra of the TiO_2 thin films at 10 K. Under the excitation above the band edge, the broad luminescence band is observed at 2.23 eV. The band shape and peak energy are similar to those of the anatase TiO_2 crystals reported previously [3, 4]. The excitation spectrum for the luminescence exhibits the response rising sharply from 3.32 eV, which corresponds to the rise on the absorption spectrum of the TiO_2 thin film. In the energy region from 3.5 to 7.0 eV, the excitation spectrum has no remarkable structure and an almost constant response.

It should be noted that the small peak around 7.8 eV and the increase of intensity with increasing photon energy from 8.0 eV are observed in the excitation spectrum above 7.0 eV. The absorption spectra calculated by K-K transformations demonstrate the absorption peak around 9.0 eV and the decrease of the ab-

sorption coefficient with increasing photon energy from 9.0 to 12.0 eV. This fact implies that the increase of the excitation spectrum from 8.0 eV is not attributed to that of the light intensity absorbed in the sample. The increase of the excitation spectrum would come from the change of the relaxation processes. In order to make the relaxation processes clear, the optical measurements over the VUV energy region are needed for the anatase TiO_2 single crystals.
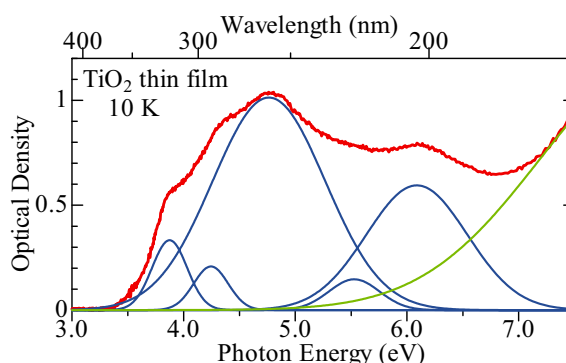
Fig. 1. Absorption spectrum (red) of the TiO_2 thin film, Gaussian components (blue) decomposing the absorption spectrum, and the background (green) consisting of the absorption tail and the substrate.
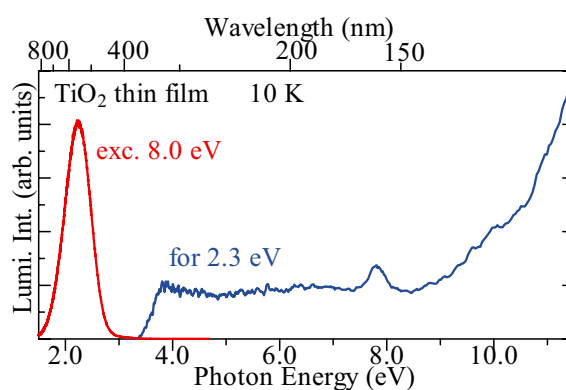
Fig. 2. Luminescence (red) and excitation (blue) spectra of the TiO_2 thin film at 10 K.

[1] A. Fujishima *et al*., Surf. Sci. Reports. **63** (2008) 515.
[2] N. Hosaka *et al*., J. Phys. Soc. Jpn. **66** (1997) 877.
[3] T. Sekiya *et al*., J. Lumi. **108** (2004) 69.
[4] M. Watanabe *et al*., J. Lumi. **112** (2005) 88.

Ⅲ-4. SURFACE AND THIN FILMS

Field Effect on the Electronic States of Pentacene Thin Films Studied by Fluorescence-Yield X-Ray Absorption Spectroscopy

H. S. Kato[1], F. Yamauchi[1, 2], M. Kawai[1, 2], H. Yamane[3], M. Nagasaka[3],
T. Hatsui[4] and N. Kosugi[3]

[1]*RIKEN (The Institute of Physical and Chemical Research), Wako 351-0198, Japan*
[2]*Department of Advanced Materials Science, University of Tokyo, Kashiwa 277-8501, Japan*
[3]*Institute for Molecular Science, Okazaki 444-8585, Japan*
[4]*PRESTO, JST and XFEL Project Head Office, RIKEN, Sayo 679-5148, Japan*

Introduction

In order to extend new functionality of electronic devices, the molecular devices have recently been investigated with great efforts. The organic field effect transistor (OFET) is a typical molecular device that controls electric conductivity by injection of carriers into the organic thin film under the applied electric field. Since the organic materials consist of molecular units having their own molecular orbitals, it is not clear that the energy diagram of OFET is exactly the same as that of the inorganic semiconductors, i.e., band bending at the interface in the semiconductor side. Therefore, the direct observation of electronic states in the organic thin films under operative conditions has been required.

In this study, we aim to elucidate the electronic state of organic thin films in OFET under the electric field. The fluorescence-yield X-ray absorption spectroscopy (FY-XAS) should be a promising method for detection of inner electronic states of organic devices, because the fluorescent X-ray has a long penetration depth of about 100 nm in most of materials even for the soft X-ray region. In addition, X-rays are not disturbed by applied electric fields, different from emitted electrons. Thus, we have attempted to utilize FY-XAS for investigation of inner electronic states of OFETs.

Experimental

To investigate the electronic states of OFET, pentacene (Pn) thin films on the SiO_2-covered Si substrates were fabricated using a molecular beam deposition system at RIKEN. The quality of their morphology and crystallinity was high enough in comparison with that reported in previous work. The performance as FETs of the fabricated Pn thin films was also confirmed with additive deposition of Au electrodes (35 nm thick) on the films. By the same preparation, the fully Au-covered Pn thin-film samples were made to evaluate the field effects under uniform electric fields in the films.

The FY-XAS measurements were performed at the BL3U beamline of the UVSOR facility in IMS. The samples were set in a BL3U end-station through a sample-entry system. The fluorescence intensities were measured using a retarding field detector consisting of MCP plates.

Results and Discussion

Figure 1(a) shows the gate bias dependence of the C K-edge FY-XAS spectra of the Pn films (20 nm thick), in which the spectra at the bias of 0 V and -90 V are plotted. The bias voltage was applied with a square wave (7 Hz) synchronized to the veto signals to the two fluorescence signal counters for each of the bias conditions, which enabled reliability of the difference spectrum. Figure 1(b) shows the spectral change at the biases from 0 V to -90 V, in which the sharp peaks at the photon energies around 285 eV on the spectra are absent, while broad components are found at the higher photon energies. In Fig. 1(b), the spectral change of a Pn-lacked sample at the same bias conditions is also shown. Although a small fluctuation possibly originates from imperfection of X-ray intensity monitoring, no meaningful signals were confirmed. It is, therefore, concluded that the observed spectral change is caused by an electronic change of the Pn thin films in FET under the applied bias, though its origin has been under debate.
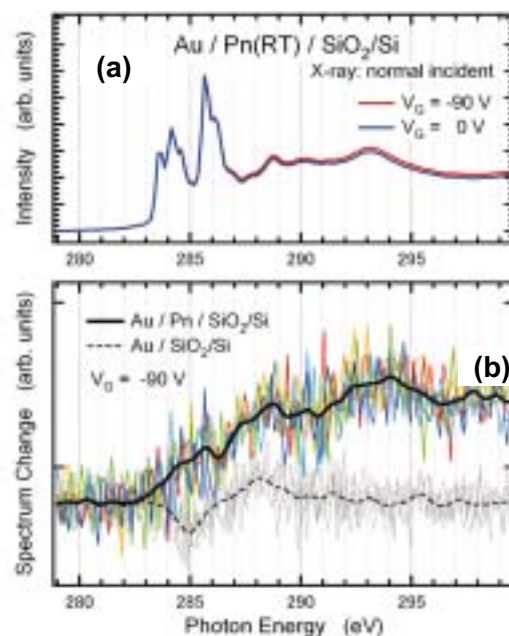
Fig. 1. Bias dependence of the C K-edge fluorescence-yield XAS spectra of the Au-covered Pn films (20 nm thick) measured at normal incidence geometry: (a) the spectra at the biases of 0 V and -90 V, (b) spectral changes at the biases form 0 V to -90 V (solid lines) as compared with that of a Pn-lacked sample (broken lines).

Synchrotron-Radiation-Stimulated Etching of PDMS Using XeF$_2$ as Reaction Gas

T.-C. He[1], T. Makimura[2], S. Torii[2], T.-Y. Chiang[3], R. Tero[3], C.-S. Wang[1] and T. Urisu[3]

[1]*Department of Physics, Shanghai Jiao Tong University, Shanghai 200240, China*
[2]*Institute of Applied Physics, University of Tsukuba, Tsukuba 305-8573, Japan*
[3]*Institute for Molecular Science, Okazaki 444-8585, Japan*

PDMS elastomer is used in many applications including micro fluidic circuits, insulation or micro/nanoelectro-mechanical (MEMS) devices and soft lithography, and it is also biocompatible and effective for fluid seals. The ability to reliably pattern PDMS in the form of both thick substrates and thin membranes or films is critical to expand the scope of its applications. In the past years, many methods for patterning PDMS have been developed, such as molding method, wet chemical etching, dry (plasma) etching, photolithography and bond-detach lithography. However, these methods can be only applicable to very thin PDMS membranes. We think that development of reliable removing type microfabrication technique applicable to thick PDMS membranes is an important issue and this will realize new 3D microstructures of PDMS by combining with molding type technique. In this work, high speed SR etching beam line using XeF$_2$ as reaction gas has been constructed (Fig.1) and high spatial resolution, area selective and anisotropic etching of elastic material PDMS has been demonstrated for the first time. Extremely high etching rate of 40-50 µm/10 min was easily obtained (Fig.2) at the XeF$_2$ gas pressure of 0.2-0.4 Torr. This suggests that SR etching using XeF$_2$ gas provides a new microfabrication technology for thick PDMS membranes. Figure 3 shows the optical microscope image of the patterning formed on the PDMS substrate surface by the SR etching under the conditions of 0.4 Torr XeF$_2$ gas and 110 mA ring current. In our following plan, the research will be extended to apply the etched surface structures to the 3D microstructures biosensor.

Fig. 2. Observed dependence of etched depth on XeF$_2$ pressure of 0.35, 0.2 and 0.1 mTorr. These data show that a high speed, area selective and anisotropic etching is realized for PDMS by the SR etching using XeF$_2$ as an etching gas.
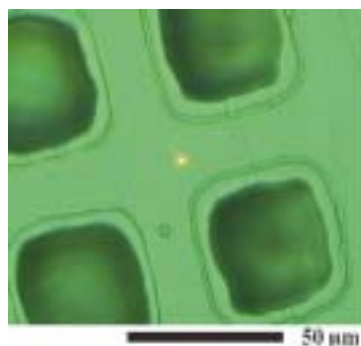
Fig. 3. The optical microscope image of the pattern formed on the PDMS by the SR etching using XeF$_2$ as reaction gas.

Fig. 1. Schematic diagram synchrotron radiation XeF$_2$ etching beam line at UVSOR. LS: light source, FCV: fast closing valve, FM1, FM2: first and second focusing mirrors, FMC: second focusing mirror chamber, DPi (i = 1 - 3): differential pumping chambers, IPi (i = 1 - 2): ion pumps, TMPi (i = 1 - 4): turbo molecular pumps, EC: etching chamber, A: aperture. Distances from the light source are written in the figure.

Ⅲ-4. SURFACE AND THIN FILMS

Evaluation of Magnetism of MnSi Ultra-Thin Films on Si(111)

S. Higashi[1], Y. Takagi[2], T. Nakagawa[2], T. Yokoyama[2] and H. Tochihara[1]

[1]Department of Molecular and Material Sciences, Kyushu University. Kasuga 816-8580, Japan

[2] Institute for Molecular Science, Okazaki 444-8585, Japan

We report on a study of surface magnetism of MnSi ultra-thin films on Si(111) by means of X-ray magnetic circular dichroism (XMCD) at BL4B, equipped with a superconducting magnet system.

It has been revealed that the deposition of Mn atoms on the Si(111)-7×7 surface at room temperature (RT) followed by subsequent annealing at elevated temperature results in the Volmer-Weber type growth of a manganese silicide [1]. The structure of the silicide is considered to be the B20 type structure of MnSi, based on results of photoemission spectroscopy and transmission electron microscopy studies.

Recently, we reported a recipe for fabrication of atomically flat MnSi ultra-thin films on Si(111) : 3ML (ML; 1ML = 7.83×10^{14} atoms/cm^2) of Mn deposition at RT followed by subsequent annealing at relatively low temperatures (~250°C) [2]. According to recent DFT calculations, the ferromagnetic ordering is slightly more stable than other magnetic structures. In addition, the structure has 50% of spin polarization at the Fermi level [3].

In this study, we grew the atomically flat MnSi ultra thin-film and evaluated the surface magnetism of the film. Samples were prepared in the preparation chamber, and then transferred to the XMCD measurement chamber under ultra-high vacuum conditions ($< 3\times10^{-10}$ Torr).

First, we measured XAS spectra of Mn $L_{III,II}$-edge under the magnetic field of 5 T at a sample temperature of 5 K with different light incident angles (0° and 55°) for the sample of Mn-3ML. For both incident angles, weak MCD signals were observed. The XAS and XMCD spectra for Mn $L_{III,II}$-edge at an incident angle of 55° are shown in Fig. 1.

In order to know the magnetic easy axis of the MnSi film, the dependence of Mn L_{III}-edge intensity under the external magnetic field up to ±5T was measured. The magnetization was not saturated at an incident angle of 0° even under 5 T, while it was saturated around 2 T at 55° incident angle (see Fig. 2). Thus we conclude that the magnetic easy axis of MnSi of Mn-3ML is in-plane.

Then, we increased the Mn amount to 10 ML and measured XAS and XMCD spectra. The XMCD signal for Mn-10ML was as weak as the sample of Mn-3ML. Additionally, The M-H curve recorded as Mn L_{III} XAS intensity indicated that the magnetic easy axis was in-plane. These results imply the magnetic moment of MnSi thin-film is independent of the thickness of the film up to 10 ML.
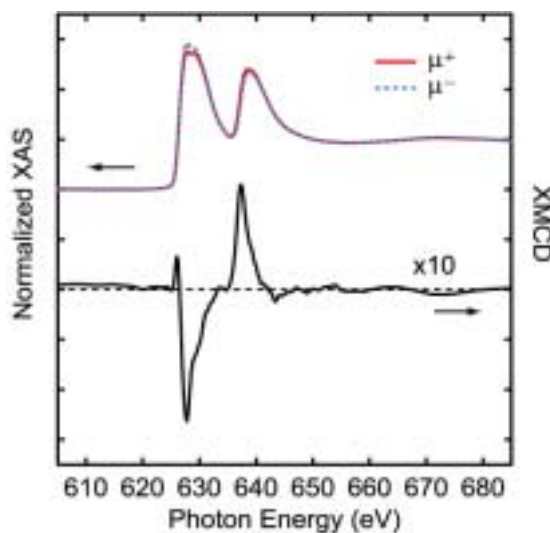
Fig. 1. Mn $L_{III,II}$-edge circularly polarized X-ray absorption spectra (blue and red lines) and XMCD spectrum (black line) of the Mn-3ML MnSi film on Si(111) at 5 K with light incident angle of 55°. μ^+ and μ^- denote those for the X-ray helicities parallel and anti-parallel to the electron spins in the specimen, respectively.
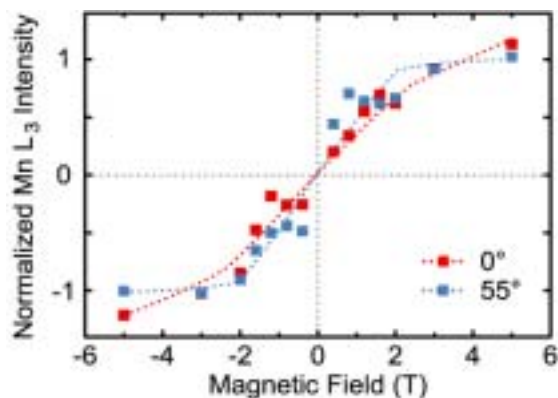
Fig. 2. M-H curves for Mn-3ML at 5.0 K, recorded as Mn L_{III} XAS intensity. The light incident angles were 0° (red) and 55° (blue). The signals were normalized by the intensity at an incident angle of 55° under 5 T. The dotted lines were drawn for eye guide.

[1] M. M. R. Evans, J. C. Glueckstein and J. Nogami, Phys. Rev. B **53** (1996) 4000.

[2] S. Higashi, Y. Ikedou, P. Kocán and H. Tochihara, Appl. Phys. Lett. **93** (2008) 013104.

[3] M. Hortamani, P. Kratzer and M. Scheffler, Phys. Rev. B **76** (2007) 235426.

Spin-Dependent Transport in Codeposited C_{60}-Co Films with Giant Tunnel Magnetoresistance

Y. Matsumoto[1], S. Sakai[1], Y. Takagi[2], T. Nakagawa[2] and T. Yokoyama[2]

[1]*Advanced Science Research Center, JAEA, Tokai, Naka 319-1195, Japan*
[2]*Institutes for Molecular Science, Okazaki 444-8585, Japan*

The spin transport in the organic molecule-based materials has attracted for its capabilities in the spintronics fields, and several groups have reported significant magnetoresistance (MR) effects in the hybrid systems of the π-conjugated molecules and ferromagnetic transition metals. In particular, the large tunnel magnetoresistance (TMR) effects were found for the granular C_{60}-Co films consisting of a C_{60}-Co compound matrix and Co nanoparticles [1]. However, the mechanism of these MR effects have not been clarified due to the absence or limited insights into the electronic and spin states essential for the magnetotransport properties.

In the present study, the electronic and spin states of the C_{60}-Co films are investigated by employing the X-ray absorption spectroscopy (XAS) and magnetic circular dichroism (MCD) measurements.

XAS and MCD measurements were carried out in the TEY mode at the magic angle. For the MCD measurements, the magnetic field (H) was applied parallel and antiparallel to the propagating direction of the circularly polarized X-ray (P_c=0.80±0.03) by using a superconducting magnet [2]. C_{60}-Co films (30nm thick) with the different Co contents (C_{60}Cox, x: the number of Co atom per a C_{60} molecule) were prepared with the codeposition method under the UHV condition (<10^{-7}Pa) [1]. The prepared samples were transferred into the analysis chamber without breaking the UHV condition.

Figure 1(a) and (b) show the Co $L_{3,2}$-edge XAS spectra of C_{60}Co$_{4.3}$ sample which corresponds to the C_{60}-Co compound [3], and the MCD spectra of the respective samples measured at T=6K under H=50kOe, respectively. Fig. 1(c) and (d) show the H-dependence of the spin and orbital magnetic moments (M_{spin} and M_{orb}). The T-dependence of the total magnetic moment (M_{tot}=M_{spin}+M_{orb}) are also shown in Fig. 2(a).

For the C_{60}Co$_{4.3}$ sample, the peak of the MCD spectrum is observed close to the characteristic energy position to the C_{60}-Co compound (A_0 resonance). The magnitude of the M_{tot} exhibits a strong T-dependence, which is roughly proportional to the inverse of the temperature. These results indicate the paramagnetic-like spin-polarization of the Co 3d-derived states in the C_{60}-Co compound.

Figure 2(b) shows the T-dependences of the zero-bias MR ratios (MR$_0$) for the granular C_{60}–Co films, and of the model-calculated MR ratios (MR$_{calc}$) as shown in the following. By virtue of the Julliere's model, the MR ratio is given as MR$_{calc}$=$m^2P^2/(1+m^2P^2)$ in case of the granular

systems, where P denotes the spin-polarization of tunneling electrons and m=M/M_S (M: magnetization, M_S: saturation magnetization). In the present work, MR$_{calc}$ is calculated by substituting m with m=M_{tot}(50kOe)/M_{sat} for the C_{60}Co$_{4.3}$ sample and by assuming $P≈1$ in consideration of the remarkably high MR ratios. As shown in the figure, the MR$_{calc}$–T dependence is found to agree well with the MR$_0$–T dependences of the granular C_{60}–Co films. This suggests that the spin-polarized Co 3d-derived states in the C_{60}–Co compound affect on the spin-dependent tunneling process. We speculate that the high spin-polarization of the tunneling electrons is induced at the interfaces of the spin-polarized C_{60}–Co compound and Co nanoparticles.
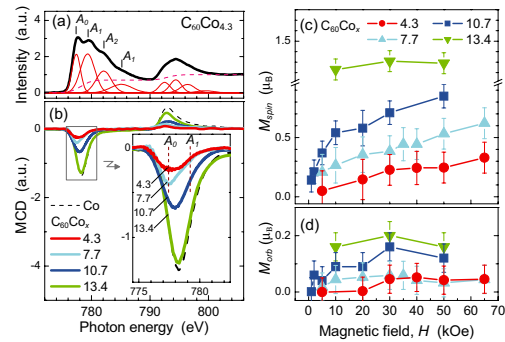
Fig. 1. (a) The Co $L_{3,2}$-edge XAS and MCD spectra of the C_{60}Co$_{4.3}$ sample, and (b) the MCD spectra of the respective samples measured at T=6K under H=±50kOe. The H-dependences of the (c) spin and (d) orbital magnetic moments (M_{spin} and M_{orb}).
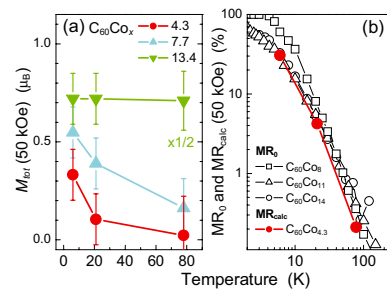
Fig. 2. (a) Temperature dependences of the total magnetic moment (M_{tot}) for the C_{60}-Co films, and (b) the zero-bias MR ratios (MR$_0$) under H=±50kOe and the model calculated MR ratios (MR$_{calc}$).

[1] S. Sakai *et al.*, Appl. Phys. Lett. **91** (2007) 242104.
[2] T. Nakagawa *et al.*, Jpn. J. Appl. Phys. **47** (2008) 2132.
[3] S. Sakai *et al.*, Thin Solid Films **515** (2007) 7758.

Ⅲ-4. SURFACE AND THIN FILMS

Magnetic Properties of Iron Nitride Thin Films on Cu(001)

Y. Takagi[1, 2], K. Isami[2], I. Yamamoto[1], T. Nakagawa[1, 2] and T. Yokoyama[1, 2]

[1]*Institute for Molecular Science, Okazaki, Aichi 444-8585, Japan*
[2]*The Graduate University for Advanced Studies, Okazaki, Aichi 444-8585, Japan*

We report on a study of the surface magnetism of iron nitride thin films on Cu(001) by means of X-ray magnetic circular dichroism (XMCD) at BL4B, equipped with a superconducting magnet systems.

The iron nitride films on Cu(001) were prepared as follows. First, The Cu(001) single crystal was cleaned by Ar^+ ion sputtering and 900K annealing cycles in ultrahigh vacuum (UHV) chamber. Next, 1ML Fe was deposited on the substrate at room temperature (RT). Then, the 1ML Fe film was exposed to low energy (150eV) N^+ bombardment with pressure = 5×10^{-6} Torr at RT for 15 min. Finally, the 1 ML iron nitride film was formed after annealing the sample in UHV at 670K for 10min. The deposition and annealing processes were repeated for more than 1ML.

The results of scanning tunneling microscopy and low energy electron diffraction studies revealed that the iron nitride films epitaxially grew on the Cu(001) substrate with the surface structure of *p4gm*(2×2). The 1ML thickness film have a 2:1 Fe:N composition, where the N atoms locate at fourfold hollow site of 1ML fcc Fe on Cu(001). On the other hand, the Fe:N composition is 4:1 for more than 1ML film. These films have the similar structure as the bulk γ-Fe_4N.

Figure 1 gives magnetization curves obtained by recording the electron yield with the photon energy fixed at the Fe L_{III} peak top (~707 eV). The spectra for the grazing incidence (θ=55°) had the step-like shape, while the smoothed shape of the magnetization curves appeared for the normal incidence (θ=0°). Therefore, the magnetic easy axis was found to be in-plain. Moreover, the magnetization at normal incidence was not saturated even under 5 T in 1ML and 2ML, while that of more than 2ML film was saturated around 3 T, as the result of decreasing the magnetic anisotropy with increasing the thickness.

The XMCD spectra of Fe $L_{III,II}$-edge were measured under the magnetic field of 5 T at a sample temperature of 5 K (Fig. 2). The spin (m_{spin}) and orbital (m_{orb}) magnetic moments obtained by each experimental XMCD spectra are indicated in the figure. Because the magnetization of 1ML and 2ML was not saturated even at 5 T at normal incidence, the spin and orbital magnetic moments of them were obtained by the spectra of the magic angle arrangement (θ=55°). On the other hand, the in-plane and perpendicular orbital magnetic moments ($m^{\parallel}_{orb}$ and $m^{\perp}_{orb}$) were analyzed for the spectra of 3ML and 4ML. The spin magnetic moment increases with increasing the thickness and is saturated at $1.8\mu_B$ around 3ML. In addition, the total magnetic moment is almost the same as the bulk γ-Fe_4N of $2.2\mu_B$.
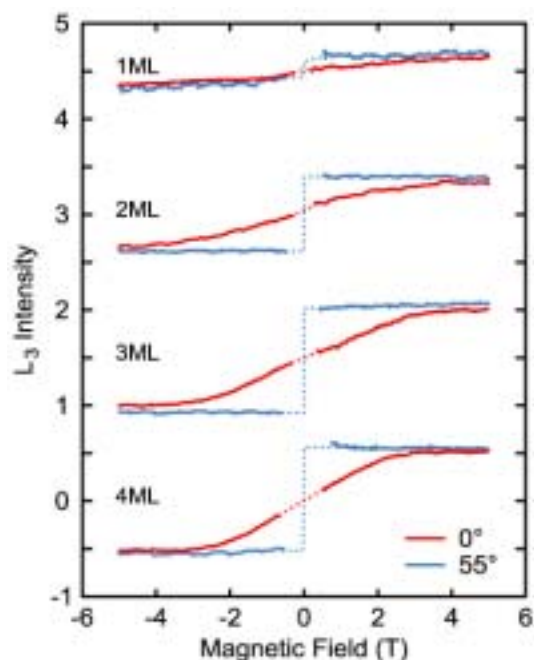
Fig. 1. The M-H curve of 1 - 4 ML iron nitride films obtained by recording the electron yield with the photon energy fixed at the Fe L_{III} peak top (707 eV) at incident angles θ = 0° (red line) and θ = 55° (blue line) from the surface normal.
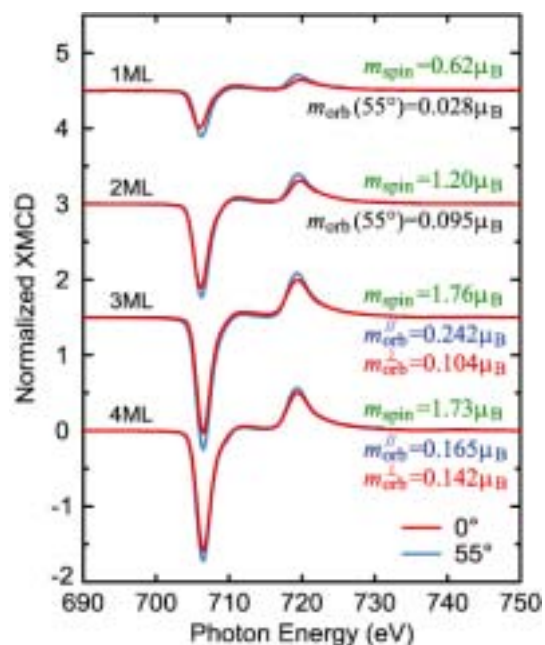
Fig. 2. Fe L_{III-II}-edge XMCD spectra of 1 - 4 ML iron nitride films under H = ±5.0T at incident angles θ = 0° (red line) and θ = 55° (blue line), normalized with the $L_{III,II}$-edge jump.

Spin Reorientations of Fe/Ni/Pd(111) Films Studied by XMCD

I. Yamamoto, T. Nakagawa, Y. Takagi and T. Yokoyama

Institute for Molecular Science, Okazaki 444-8585, Japan

Surface magnetic anisotropy of magnetic thin films is one of the critical factors in determining the magnetization easy axis. The surface anisotropy is sensitive to surface modifications such as the adsorption of gases and metals, which induce sometimes spin reorientation transition (SRT). In this work, we have investigated Fe-induced SRTs for Ni/Pd(111) system by x-ray magnetic circular dichroism (XMCD).

Fe and Ni thin films were prepared by electron-beam evaporation method at room temperature. The angle-dependent Fe L-edge and Ni L-edge XMCD measurements were performed with a total electron mode using a UHV-compatible superconducting magnet (7 T) XMCD system with a liq. He cryostat [1]. The XMCD spectra were recorded with reversal of magnetic field, and using the circularly polarized synchrotron radiation. All XMCD measurements were done at 55 K.

Figure 1 shows magnetization curves for various Fe thicknesses on Ni(6 ML)/Pd(111) along the surface normal, recorded with the Ni L_{III} XMCD intensity. The magnetic fields of ±5 T are thus confirmed to be enough to saturate the magnetization even along the hard axis. The magnetization easy axis of Ni/Pd(111) system, which shows no thickness-driven SRT, is in-plane. By depositing Fe, two opposite SRTs was observed. Initially submonolayer Fe deposition causes a transition to perpendicular magnetization, and further Fe deposition (~3 ML) induces a return transition to in-plane magnetization. The anisotropic magnetic fields H_a were 0.8 T and 1.8 T for Fe 3 ML and 0 ML (bare Ni 6 ML), respectively (Fe 1 ML and 2 ML is the easy axis). The effective magnetic anisotropy energy K^{eff} were obtained as -38 μeV/atom (Fe 3ML) and -25 μeV/atom (bare Ni 6 ML).

The angular dependent Ni $L_{III,II}$-edge and Fe $L_{III,II}$-edge XMCD spectra for Fe/Ni(6 ML)/Pd(111) at T= 55 K and H= 5 T are shown in Fig. 2. All the XMCD spectra are normalized at L_{II}-edge. The orbital magnetic moments (perpendicular: $m_{orb}^{\perp}$, in-plane: $m_{orb}^{//}$) and spin magnetic moments m_{spin} were obtained by applying the sum rule. The obtained orbital magnetic moments of both Ni and Fe along the magnetization easy axis are larger than that of the hard axis. This result indicates that the orbital magnetic moments contribute to determining the magnetization easy axis.

[1] T. Nakagawa, Y. Takagi, Y. Matsumoto and T. Yokoyama, Jpn. J. Appl. Phys. **47** (2008) 2132.
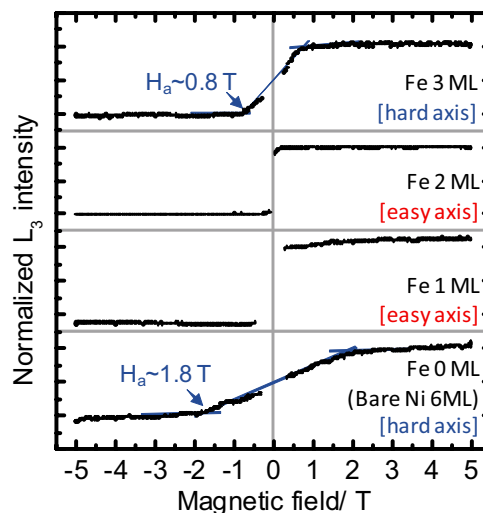
Fig. 1. Magnetization curves of Fe(0-3 ML) on Ni(6 ML)/Pd(111) at 55 K, recorded as Ni L_{III} XMCD intensity.
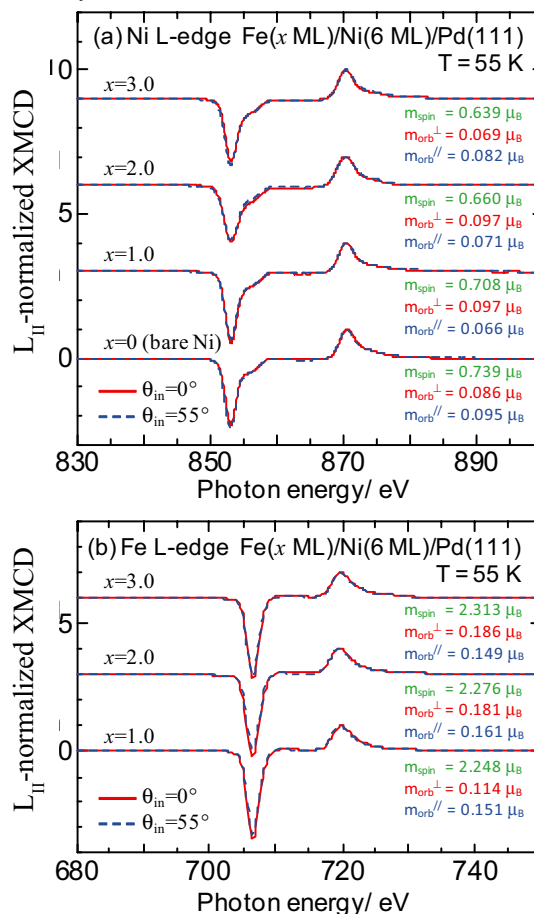
Fig. 2. XMCD results for Fe/Ni(6 ML)/Pd(111). (a) Ni L-edge XMCD spectra. (b) Fe L-edge XMCD spectra.

Ⅲ-4. SURFACE AND THIN FILMS

Angular Dependent XMCD Study of Perpendicularly Magnetized Fe$_{1-x}$Co$_x$/Rh(001)

F. Yildiz[1], M. Przybylski[1], Y. Takagi[2], T. Nakagawa[2], I. Yamamoto[2] and T. Yokoyama[2]

[1]*Max-Planck-Institut für Mikrostrukturphysik, Weinberg 2, 06120 Halle, Germany*
[2]*Institute for Molecular Science, Okazaki, 444-8585, Japan*

Perpendicular magnetic anisotropy is one of the most important subjects in thin film magnetism because of its technological requirements and fundamental interest in physics. Recently, Yildiz *et al*. [1] discovered extremely strong perpendicular magnetic anisotropy in Fe$_{1-x}$Co$_x$ alloy films on Rh(001). The maximum critical thickness achieves as much as 15 monolayer (ML) when x=0.6. It was speculated from the remanent XMCD measurements that the orbital magnetic moment of Co dominantly contributes to magnetic anisotropy. In this work, we have measured *in situ* Fe and Co L-edge XMCD (x-ray magnetic circular dichroism) spectra using a superconducting magnet (±7 T) and a liq. He cryostat.

The experiments were carried out at BL4B. Fe and Co were codeposited on clean Rh(001). The concentration ratio Fe:Co was determined by the Fe and Co edge jumps. The XMCD spectra were taken at H=±5 T and T=4.9 K with the incidence angles θ_{in} of 0° (normal incidence) and 55°. The helicity of the x-rays was fixed positively (P_c=+0.67), while the magnetic field was reversed.

The XMCD spectra shown in Figs. 1 and 2 were analyzed using the well-known sum rules. The orbital magnetic moments $m_{orb}(\theta_{in})$ and the effective spin magnetic moments $m_{spin}^{eff}(\theta_{in})$ obtained experimentally yielded the perpendicular and in-plane orbital magnetic moments $m_{orb}^{\perp}$ and $m_{orb}^{//}$, the magnetic dipole moments $m_T^{\perp}$ and $m_T^{//}$, and the intrinsic spin magnetic moment m_{spin}.

The obtained perpendicular and in-plane orbital magnetic moments $m_{orb}^{\perp}$ and $m_{orb}^{//}$ are found to be quite large in both Fe and Co. Especially, it should be noted that the orbital magnetic moments of Fe are large, although the bulk Fe shows much smaller orbital magnetic moment. Moreover, Fe shows more significant angular dependence of the orbital magnetic moment, implying that the strong perpendicular magnetic anisotropy originates mainly from the Fe orbital magnetic moment of Fe, not from the Co one. The present work successfully demonstrates the importance of the hard-axis measurement at a sufficiently high magnetic field using a superconducting magnet for the discussion of magnetic anisotropy.

[1] F. Yildiz, F. Luo, C. Tieg, R. M. Abrudan, X. L. Fu, A. Winkelmann, M. Przybylski and J. Kirschner, Phys. Rev. Lett. **100** (2008) 037205.
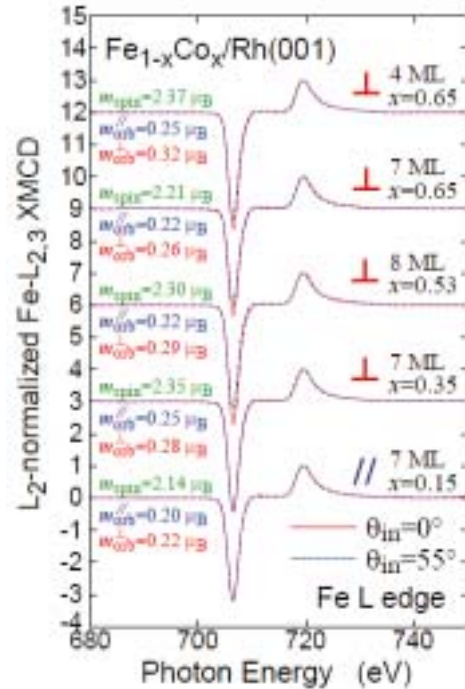
Fig. 1. Fe L-edge XMCD of Fe$_{1-x}$Co$_x$/Rh(001) at H=±5 T and T=4.9 K. "⊥" and "//" imply that the corresponding films show the perpendicular and in-plane easy axes, respectively.
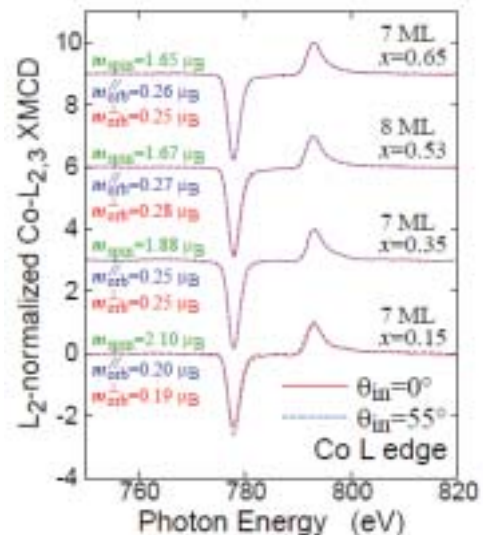
Fig. 2. Co L-edge XMCD of Fe$_{1-x}$Co$_x$/Rh(001) at H=±5 T and T=4.9 K.

BL7B

VUV Reflection Spectroscopy of PdO, PtO and $Pt_{1-x}Pd_xO$ Thin Films

Y. Iwai, K. Nakagawa, T. Mizunuma, T. Yabumoto, Y. Takayanagi,
S. Matsumoto and H. Matsumoto

School of Science & Technology, Meiji University, Kawasaki 214-8571, Japan

Both PdO and PtO have the same crystal structure and atomic coordinate, and extremely near lattice constants. Extensive experimental and theoretical studies have been performed for the electronic structures of PdO [1]. On the other hand, there are a few reports for PtO in experimental data obtained by electric and optical measurements. Various reports have been done about the existence of the band gap of PtO. In recent yeas, a small gap was expected [2]. To verify the result of the theoretical results, we try to take a wide view of the electronic structure of PtO by obtaining a wide range optical properties experimentally. As part of this work, we designed to use PdO as an object of comparison of PtO [3]. In the present study, $Pt_{1-x}Pd_xO$ thin films were prepared, and they were added to the target for comparison.

Experiment

$Pt_{1-x}Pd_xO$ thin films ($0 \leq x \leq 1$) were deposited by RF reactive sputtering on fused quartz substrate, at a temperature of 673 K. Metal palladium and platinum plate were used as the target, and the sputtering was carried out in argon and oxygen mixture gases. The film thickness was about 150 nm. Composition ratio, chemical bonding states and crystallinity of the films were investigated by RBS, XPS and XRD.

Reflection spectra of the films were measured under the vacuum ultraviolet region up to 30 eV with the 3-m normal incident monochromator (grating: G1 and G2) at BL-7B of UVSOR-II. And a silicon photodiode sensor was used as a detector for the reflection light.

Results and Discussion

According to the analysis techniques mentioned above, all the films prepared for this work ware composed of polycrystalline of $Pt_{1-x}Pd_xO$.

Figure 1 shows the reflection spectra of $Pt_{1-x}Pd_xO$ thin films in room temperature. In the reflection spectra of PdO and PtO, many similar features were seen and some possibility about the relation between the peaks of PdO and PtO remained: 6 eV-peak in PdO (peak-B) is related to 4 eV-peak or 8 eV-peak in PtO; 19.4 eV-peak in PdO (peak-E) is related to 17.5 eV-peak or 21 eV-peak in PtO.

As Pt composition ratio is increased in $Pt_{1-x}Pd_xO$ thin films, peak-B and peak-E exhibited continuous shift to lower energy. Hence, it may be concluded that peak-B and peak-E in PdO are related to 4 eV-peak and 17.5 eV-peak in PtO, respectively, and peak-C in PdO is related to 8 eV-peak in PtO. Since the relations of the peaks become clear, it is possible to discuss the differences of the features of each reflection spectrum.
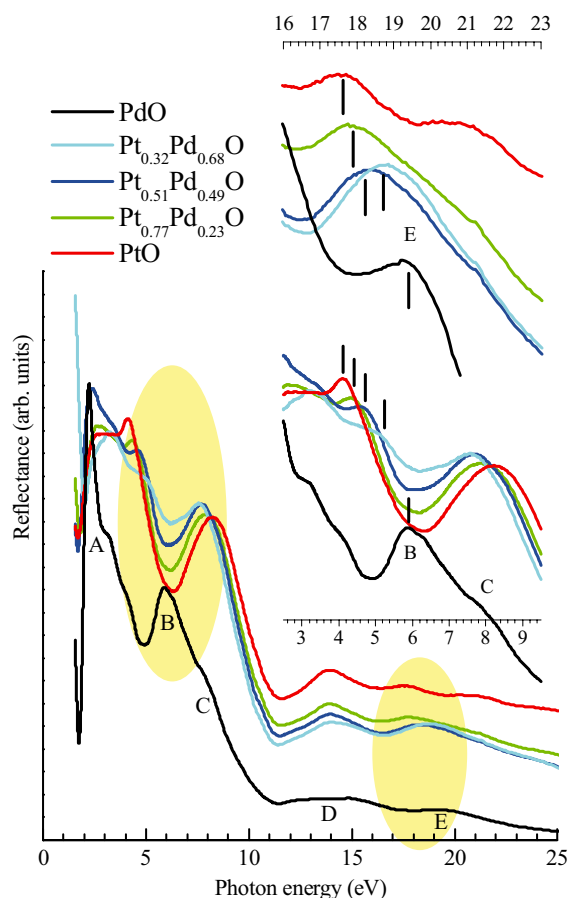
Fig. 1. Reflection spectra of $Pt_{1-x}Pd_xO$ thin films. The data below 6 eV in photon energy was measured elsewhere with deuterium and xenon lamps. The insets are expanded spectra in specific range.

The energy positions of peak-B and related peak in PtO is remarkable. In the spectrum of PdO, it is separated from peak-A by a dip. On the other hand, 4 eV-peak in PtO overlaps the reflection band below the peak. Our theoretical calculation [3] have predicted that the energy levels of Pd5s and Pd5p orbital will form at higher energy than unoccupied Pd4d orbital, and the energy levels of Pt6s and Pt6p orbital will overlap the energy levels of Pt5d orbital. Therefore, the origin of the reflection peak-B and corresponding peak in PtO is considered to be the metal s and p orbital.

[1] H. A. E. Hagelin *et al.*, J. Electron. Spectrosc. Relat. Phenom. **124** (2002) 1.
[2] J. Uddin *et al.*, Phys. Rev. B **71** (2005) 155112.
[3] Y. Iwai *et al.*, UVSOR Activity Report **35** (2008) 96.

III-4. SURFACE AND THIN FILMS

Photoabsorption Cross Section of C_{70} Thin Films from the Visible to Vacuum Ultraviolet

H. Yagi[1], K. Nakajima[1,2], K. R. Koswattage[3], K. Nakagawa[3], H. Katayanagi[1] and K. Mitsuke[1]

[1]*The Institute for Molecular Science and Graduate University for Advanced Studies, Okazaki 444-8585, Japan*

[2]*Science Research Center, Hosei University, Chiyoda-ku, Tokyo 102-8160, Japan*

[3]*Faculty of Human Development, Kobe University, Nada-ku, Kobe 657-8501, Japan*

Since Krätschmer *et al*. established the method for synthesizing macroscopic amount of C_{60} and C_{70}, optical properties of solid C_{70} have been studied by various techniques. But to our knowledge these studies were restricted to the photon energies below 6.2 eV. In the present study, we have determined the absolute photoabsorption cross section of C_{70} thin film from 1.3 to 42 eV.

Polycrystalline C_{70} films with the thickness of 11 to 57 nm were prepared by the vacuum deposition method. The collodion thin film substrate and a surface thickness monitor (Inficon, XTM/2) were mounted 90mm above the C_{70} vapor source so that their centers were equidistant from the vapor source. Thus the thickness t of the C_{70} film on the substrate was calculated from $t = M_{TM}/A_{TM}\rho$, where M_{TM} is the total mass of C_{70} deposited on the thickness monitor, A_{TM} is the effective area of the thickness monitor and $\rho = 1.68$ g cm^{-3} is the mass density of solid C_{70} at room temperature.

Optical absorption measurements were carried out by means of photon attenuation method. The absolute photoabsorption cross section σ_{film} of the C_{70} thin film was estimated by using the Lambert-Beer law.

$$\sigma_{film} = \frac{1}{tN}\ln\frac{I_0}{I} = \frac{A_{TM}M}{M_{TM}L}\ln\frac{I_0}{I}$$

Here, N is the number density of C_{70} in the sample, I is the light intensity measured downstream of the collodion substrate covered with a C_{70} film, I_0 is the light intensity measured downstream of the collodion substrate without C_{70}, L is the Avogadro constant, and M is the molar mass of C_{70}. I_0 and I were measured successively and normalized by the ring current of the storage ring.

At $h\nu < 6$ eV, present data were affected by the reflection at the sample surface and/or scattering at the grain boundaries. Therefore, instead of using present data, we calculated σ_{film} from the dielectric function $\varepsilon(\nu)$ reported by Kataura *et al*. [1] at $h\nu < 6$ eV. Thus determined σ_{film} curve is shown in Fig. 1 (black solid curve). From the σ_{film} curve in Fig. 1, we calculated the complex refractive index $n(\nu) = n'(\nu) + in''(\nu)$, and the complex dielectric function $\varepsilon(\nu) = \varepsilon_1(\nu) + i\varepsilon_2(\nu)$ by using Kramers-Kronig analysis. The $\varepsilon(\nu)$ curves obtained from present σ_{film} curve agree well with those obtained from the EELS results by Sohmen *et al*. [2].

In the case of C_{60}, the absolute photoabsorption cross section of a single molecule σ_m can be calculated from σ_{film} by considering the correction of the Lorentz-Lorenz local field by surrounding C_{60} molecules [3]. In the previous paper, we actually demonstrated that σ_m curve of C_{60} calculated from the σ_{film} curve shows good agreement with the absolute photoabsorption cross section σ_{gas} curve of gaseoou C_{60} [4]. The Lorentz-Lorenz local field correction is also applicable to our C_{70} thin films because most part of solid C_{70} prepared by vacuum deposition shows fcc structure at room temperature. The blue solid curve in Fig. 1 shows the σ_m of C_{70} calculated from present σ_{film} curve. Unlike the case of C_{60}, no experimental data of σ_{gas} of C_{70} is available above $h\nu \sim 5$ eV. Therefore we calculated σ_{gas} of C_{70} from the EELS spectrum of gaseous C_{70} [5]. Red dots in Fig. 1 represent thus calculated σ_{gas} of C_{70}, which appears to agree with the present σ_m except at several fine structures.
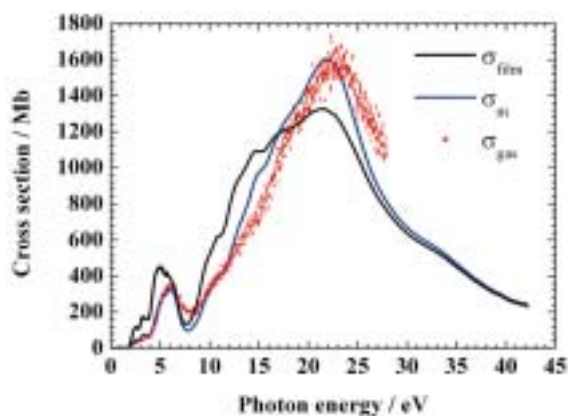
Fig. 1. Photoabsorption cross section of C_{70} thin film (black curve), C_{70} single molecule (blue curve) calculated from σ_{film}, and gaseous C_{70} (red dots).

[1] H. Kataura *et al*., J. Phys. Chem. Solids **58** (1997) 1913.

[2] E. Sohmen *et al*., Z. Phys. B: Condense. Matter **86** (1992) 87.

[3] J. Andersen and E. Bonderup, Eur. Phys. J. D **11** (2000) 435.

[4] H. Yagi *et al*., Carbon, **47** (2009) 1152.

[5] N. Ju *et al*., Phys. Rev. B **48** (1993) 9071.

Angle-Resolved UPS of Perfluoropentacene Monolayer on Graphite

S. Kera, S. Hosoumi, T. Aoki, S. Duhm, S. Nagamatsu and N. Ueno

Graduate School of Advanced Integration Science, Chiba University, Chiba 263-8522, Japan

A newly synthesized molecule of perfluoropentacene (**PFP**) was reported to act as n-channel OFET and fabricated ambipolar transistors with pentacene [1]. We have investigated the electronic structure and molecular orientation of **PFP** in a monolayer film by using angle-resolved ultraviolet photoelectron spectroscopy (ARUPS). ARUPS has been known as a powerful technique to obtain crucial information on electronic band structure for various kinds of materials. Moreover, for organic thin films, information on the geometrical structure of the thin films can be also discussed in accordance with a quantitative analysis of the ARUPS intensity using photoelectron scattering theory.

In this report, we show the observed electron-emission-angle (θ) dependence of HOMO band in ARUPS spectra for the **PFP** monolayer deposited on the graphite substrate.

Experiments

ARUPS spectra were measured at photon incidence angle $\alpha=45^o$, hν=35 eV, and T=295 K. The purified molecules were carefully evaporated onto the graphite (HOPG) substrate at 295 K. The nominal thickness of the monolayer is confirmed by the work function of the condensed monolayer film of 4.6 eV. θ dependence was analyzed using the multiple-scattering theory combined with molecular orbital calculation (MST/MO) [2]. We have calculated the θ pattern from a free molecule itself.

Results and Discussion

Figure 1 (a) shows the θ dependence of ARUPS of **PFP** (0.3nm) on the HOPG. The intensity is normalized to the incidence photon flux. A top feature appeared around 1.5 eV is ascribed to HOMO band of **PFP**. Figures 1 (c) and (d) show the comparison between observed and calculated θ dependences of the HOMO intensity. The HOMO intensities are evaluated after background subtraction and shown to normalize at the maximum intensity. The observed intensity gives the maximum at around 37°. The calculated intensities are shown for the molecular tilt angles β, which is inclined angle from the long-molecular axis, and γ, which is angle from the short axis (see Fig.1 (b)). Azimuthal angle ϕ is integrated due to the polycrystalline HOPG surface in Fig.1 (c). Among them, the molecular tilt angles of $\beta=0^o$ and $\gamma=0^o$ gives the best agreement with the observed θ pattern. However, the calculated pattern is still broader than the observed one. In Fig.1 (d), calculated θ patterns, where the patterns are obtained at fixed $\phi = 36^o$ or 38°, are compared to the observed one, giving the best agreement. It indicates that the molecules are perfectly oriented flat to the substrate

and form a uniform monolayer film, where the molecular single domain is large enough unexpectedly.

In fact, one can see a relatively large energy shift of the HOMO about 210 meV depending on the θ (see the guide lines) in Fig.1(a). The intermolecular HOMO-HOMO overlapping might be large enough to detect an energy-band dispersion. Accordingly we expect that the DOS structure in the HOMO feature of UPS, which comes from the HOMO band dispersion, could be observed even for polycrystalline **PFP** films as in pentacene standing film [3]. Note that one should also consider the large anisotropic vibronic coupling for such an ordered film. Nevertheless, ARUPS study for the well-ordered **PFP** film on the single crystal would be fascinating.
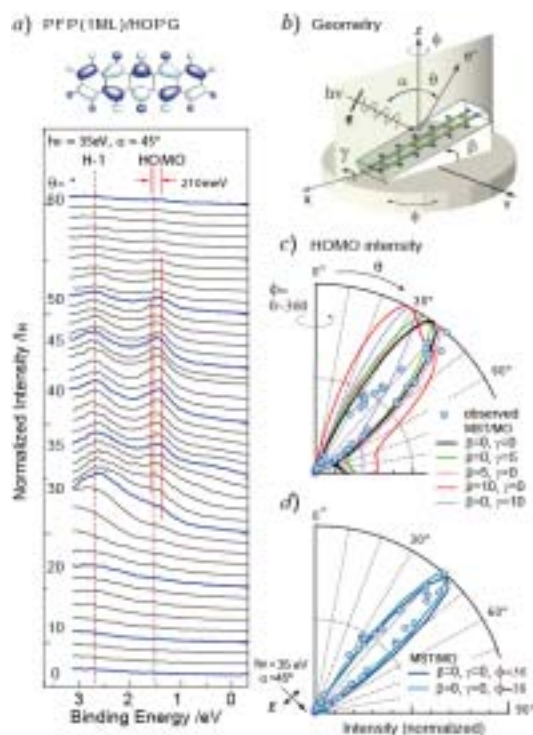
Fig. 1. (a) θ dependence of ARUPS of PFP monolayer on HOPG. (b)Computation geometry for the MST/MO method. (c) and (d) Observed and calculated θ patterns of the HOMO. ϕ is integrated for 0~360° in (c). Schematic view of the HOMO pattern is also shown.

[1] Y. Sakamoto *et al.*, J. Am. Chem. Soc. **126** (2004) 8138.

[2] S. Nagamatsu *et al.*, e-J. Surf. Sci. Nanotech **3** (2005) 461**.**

[3] H. Fukagawa *et al.*, Phys. Rev. B **73** (2006) 245310.

Ⅲ-4. SURFACE AND THIN FILMS

Electronic Structures of Single Crystalline Rubrene Studied by Photoemission Measurement Techniques

Y. Nakayama[1], S. Machida[2], T. Kubo[1, 3], A. Funakoshi[2],
N. Ogawa[3], T. Minari[4], K. Tsukagoshi[4] and H. Ishii[1, 2]

[1]Center for Frontier Science, Chiba University, Chiba 263-8522, Japan
[2] Graduate School of Advance Integration Science, Chiba University, Chiba 263-8522, Japan
[3] Faculty of Engineering, Chiba University, Chiba 263-8522, Japan
[4] National Institute for Materials Science, Tsukuba, Ibaraki 305-0047, Japan

Rubrene (5,6,11,12-tetraphenyltetracene) is one of the most promising materials for organic field effect transistor application due to its high hole mobility. To understand the transport nature and improve the device performance, information about the electronic structures is indispensable. There have been a number of reports about the electronic states of amorphous thin films (TFs) of rubrene studied by photoelectron spectroscopy (PES) [1, 2]. On the other hand, sufficiently high field effect mobility has not been realized for the rubrene TFs but only for the crystalline phase. It has been known that rubrene molecules in the single crystals (SCs) have different conformation from those in the TFs [3]. This fact implies different electronic states of rubrene SC from those of its TF phase. However, experimental observation of the electronic structures of rubrene SCs has not been reported. It is mainly because PES measurement on organic crystals has been awkward due to the sample charge-up problem.

In this study, we conducted direct observation of the electronic structures of rubrene SCs by two types of photoemission measurement techniques to overcome the aforementioned issues. The one was photoelectron yield spectroscopy (PYS) that gives us information about ionization potentials (IPs) of specimens excluding any effects of the charge-up [4]. The other was PES with special tactics, illumination of visible laser light and positive biasing on the samples, in order to relieve the charge-up problem.

Rubrene SCs were produced by a physical vapor transport technique and were fixed on conductive substrates (indium-tin-oxide (ITO) or Au) with silver paste. Rubrene TFs that were formed on ITO by *in-situ* vacuum deposition were also examined for comparison. Details of the PYS apparatus were described elsewhere [5]. PES measurement was performed at BL8B2 in UVSOR.

As shown in PYS spectra (Fig. 1), rubrene SCs exhibited apparently lower threshold energy of photoelectron emission compared to its TFs [6]. It means that crystallization lifts the highest occupied molecular orbital (HOMO) of rubrene upward to the vacuum level.

Figure 2 shows PES spectra of a SC and a TF of rubrene. Laser light (405 nm, 1 mW) and positive bias (+20 V) were applied on the SC sample during measurement. The HOMO peak of the SC appeared at a lower binding energy position compared to that of the TF, whereas positions of the other peaks are roughly same for the both spectra This result also supports the upshift of the HOMO energy of rubrene caused by crystallization. Mapping of the electronic band structures of rubrene SC by angle resolved PES is now underway by utilizing these techniques.
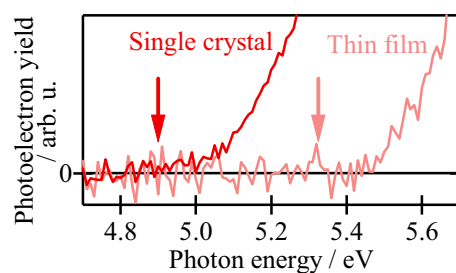
Fig. 1. PYS spectra of a SC and a TF of rubrene. Estimated IPs are indicated as arrows.
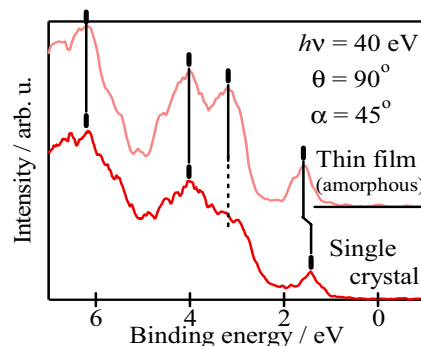
Fig. 2. PES spectra of a SC and a TF of rubrene.

[1] Y. Harada *et al.*, Chem. Phys. Lett. **62** (1979) 283.
[2] L. Wang *et al.*, Appl. Phys. Lett. **90** (2007) 132121.
[3] D. Käfer *et al.*, Phys. Rev. Lett. **95** (2005) 166602.
[4] Y. Nakayama *et al.*, Appl. Phys. Lett. **92** (2008) 153306.
[5] H. Ishii *et al.*, J. Surf. Sci. Soc. Jpn. **28** (2007) 264.
[6] Y. Nakayama *et al.*, Appl. Phys. Lett. **93** (2008) 173305.

Interaction between 11,11,12,12-Tetracyano-2,6-Naphthoquinodimethan (TNAP) and Bismuth (001)

T. Nishi[1], S. Nagamatsu[2], T. Aoki[2], K. Kato[2], S. Hara[2],
M. Tsunekawa[3], K. Sakamoto[2] and N. Ueno[2]

[1]*Center for Frontier Science, Chiba University, Chiba 263-8522, Japan*
[2]*Graduate School of Advanced Integration Science, Chiba University, Chiba 263-8522, Japan*
[3]*Research Center for Materials Science, Nagoya University, Nagoya 464-8602, Japan*

The energy level alignment at the interface between molecule and electrode is one of the most important subjects in organic thin film devices, since the phenomena at the interface such as charge injection barrier affects their performance. Complicated several factors render understanding phenomena at the interface very difficult. For example, in the case of the vacuum level (VL) shift, which is one of the most important phenomena in the energy level alignment of organic/metal interface, six factors in molecule-substrate that closely relate each other must be considered [1].

In the case of 11,11,12,12-tetracyanonaphtho-2,6- -quinodimethane (TNAP, Fig.1.), which is an electron accepter π-conjugated organic molecule shows interesting correlation on noble metal substrates. That is, a diffusion of Cu atoms to TNAP thin film, a charge transfer and a weak interaction have been observed on Cu (work function, $\Phi = 4.9$), Ag ($\Phi = 4.7$) and Au ($\Phi = 5.3$), respectively [2]. On the other hand, Bismuth is considered to be a low active material despite the low work function of its (001) surface, $\Phi = 4.22$ [3], which is smaller than those of Cu, Ag and Au. In this paper, the electronic structure of TNAP / Bi (001) is reported.

Sample was prepared by depositing TNAP (Tokyo Kasei) on a Bi(001) film formed on a Si(111)-(7×7) substrate in a ultra high vacuum chamber. The quality of the Si(111)-(7×7) reconstruction was checked by low energy electron diffraction (LEED). The thickness of Bi deposited on the Si substrate was 10 bi-layers. TNAP powder crystals were loaded in Pyrex glass crucible. The deposition rate of TNAP was less than 0.025 nm/min. UPS measurements were performed using photon energies of 21.2 eV and 50 eV. DFT calculations were carried out using the B3LYP functional, with 6-311G (p,d) and 6-311G ++ (p,d) split valence plus polarization basis set for neutral and anion state by Gaussian 03, respectively [4]. The geometry of TNAP was optimized via DFT. The angular distributions of photoemission were obtained by the multiple-scattering approximation combined with the molecular orbital (MS/MO) calculation [5].

Figure 2 shows the valence band region of UPS spectra of Bi(001) and TNAP, the thickness is ~0.3nm corresponding to 1 monomolecular layer (ML). At TNAP spectrum, a density of state was observed just below the Fermi energy like the case of 2,3,5,6-tetrafluoro-7,7,8,8-tetracyanoquinodimethane (F4-TCNQ) / Au [6]. The calculations have been done assuming that TNAP lies flat on the Bi(001) substrate by taking into account the STM image. The results indicate that the interaction between Bismuth and TNAP is strong. There is a possibility of charge transfers from Bismuth to TNAP like F4-TCNQ / Au case.
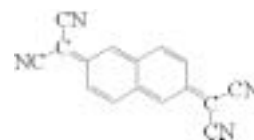
Fig. 1. Molecular structure of TNAP.
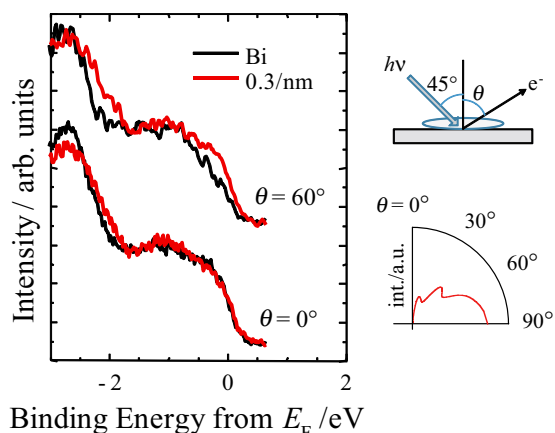
Fig. 2. UPS spectra of Bi(001) and TNAP, 1 ML, on Bi(001) and angular distribution of photoemission of TNAP- HOMO by MS/MO calculation.

[1] H. Ishii *et al.,* Adv. Mat. **11** (1999) 605.
[2] K. Kanai *et al.,* MRS symp. Proc. **871E** (2005). K. Kanai and K. Seki, J. Vac. Soc. Jpn. **50** (2007) 722.
[3] H. Kakuta *et al.,* Phys. Rev. Lett. **98** (2007) 247601.
[4] Gaussian 03, Revision C.02, M. J. Frisch *et al.*, Gaussian, Inc., Wallingford CT, 2004.
[5] S. Nagamatsu *et al.*, e-J. Surf. Sci. Nanotech. **3** (2005) 461.
[6] N. Koch *et al.*, Phys. Rev. Lett. **95** (2005) 247601.

Ⅲ-4. SURFACE AND THIN FILMS

Molecular Orientation of P3HT Thin Film by ARUPS

K. K. Okudaira, Y. Suzuki and N. Ueno

*Association of Graduate Schools of Science and Technology, Chiba Univererity,
Chiba 263-8522, Japan*

Introduction

The structure-property relationship of solution-processible conducting polymers with π-conjugated electronic structures have been explored extensively due to their significant impact in optoelectronic applications. Solution-processed regioregular conjugated poly(3-hexylthiophene) (P3HT) thin films can easily lead to well-organized conformation leading to highly oriented polymer films.[1] The long-range order and π-π interchain stacking in the P3HT thin films play an important role on the charge transport process and the device performance. However, few studies on structural characteristics such as quantitative determination of surface molecular orientation were reported.

In this report we observed angle-resolved ultraviolet photoelectron spectra (ARUPS) of P3HT spin-casted thin films with various coating parameters to clarify the molecular orientation (tilt angle of polymer backbone)

Experimental

ARUPS measurements were performed at the beam line BL8B2 of the UVSOR storage ring at the Institute for Molecular Science. The take-off angle (θ) dependencies of photoelectron spectra were measured at incident angle of photon (α) = 45° with the photon energy (hv) of 40 eV.

The polymer thin films were prepared on gold coated Si(100) wafers by spin casting.. The spin casting was performed 60s with speeds of 4500 and 400 rpm for solution concentrations of 5 and 0.5 mg/mL, respectively.

Results and Discussion

Figures 1 (a) and (b) show the θ dependencies of ARUPS spectra of P3HT thin film with speeds of 4500 and 400 rpm, respectively. In Figure 1 peak 1 located at about binding energy of 3-4 eV corresponds to the localized π states contributed from S 3pz.[2] For both sample, the intensities of peak 1 show θ dependence..

The observed θ dependencies of the peak 1 (π band) intensities of the P3HT thin film with different spin-cast speeds are plotted in Fig. 2. It was found that the θ dependence of the π band (peak 1) intensity for the thin film with spin-casted speed of 4500rpm is different from that with 400 rpm. It indicates that the molecular orientation (tilt angle of polymer backbone) was affected by process parameter. To determine the molecular orientation quantitatively, it needs to compare the observed θ dependencies with the calculated ones.

[1] H. Sirringhaus *et al.*, Nature **401** (1999) 685.
[2] X. T. Hao *et al.*, J. Phys. Chem. B. **111** (2007) 10365 .
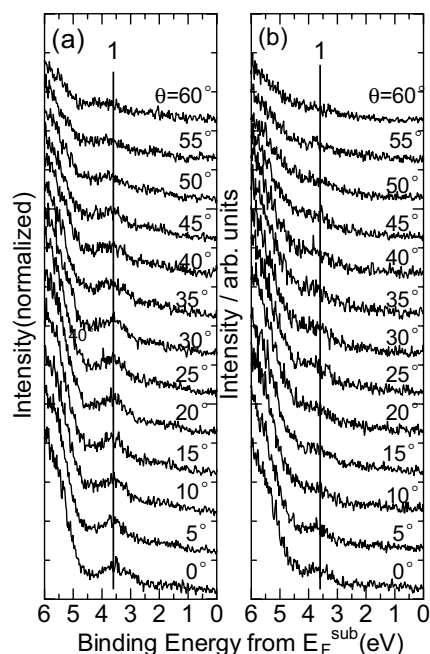
Fig. 1. Take-off angle (θ) dependence of ARUPS of P3HT spin-casted thin films with speeds of 4500 (a), 400 rpm (b), respectively.
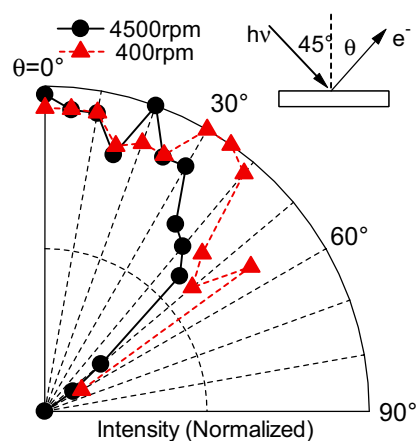
Fig. 2. Take-off angle (θ) dependencies of photoelectron intensities of peak 1 (indicated in Fig. 1) for P3HT spin-casted film with speeds of 4500 (●) and 400 rpm (▲).

Ⅲ-4. SURFACE AND THIN FILMS

Formation of Interface State at the Zinc-Phthalocyanine/In Interface

S. Tanaka, K. Watanabe, S. Mizuta and I. Hiromitsu

Department of Material Science, Interdisciplinary Faculty of Science and Engineering,
Shimane University, Matsue 690-8504, Japan

Organic electronics devices, such as organic light emitting diodes, organic solar cells, organic thin film transistor, etc…, are expected as a candidate of the electronics devices for the next generation. The property of metal/organic interface has a critical role for the performance of such organic electronics devices.

In this study, we focused on the interface electronic structure of the zinc phthalocyanine (ZnPc)/In interface. ZnPc is a semiconducting material and plays an important role in the organic devices. In has a small work function (~4.1 eV) and is used as a cathode (or electron injection) metal.

The electronic structure of ZnPc and In interface was investigated by using the photoelectron spectroscopy. Figure 1 shows photoelectron spectra of In incrementally deposited on the ZnPc layer. The abscissa is the binding energy relative to the Fermi energy of substrate. The light with photon energy of 40 eV was used for the measurements. The deposition rate of In was ~ 0.2 nm/min. The peak at 1.5 eV in the ZnPc (30 nm) spectrum is the highest occupied molecular orbital (HOMO) of ZnPc. In the spectrum of 0.5 nm of In on the ZnPc layer, an in-gap peak was observed at around 0.5 eV (The hatched area in the figure). In addition, the intensity of HOMO of ZnPc was decreased drastically with a slight shift toward higher binding energies. Similar behavior has been observed in the experiments about the In deposition on the organic layers [1, 2]. The origin of the interface states of the In-on-ZnPc interface was considered as the electron transfer from In to ZnPc by analogy with the study of In on copper phthalo-cyanine system [2]. On the secondary electron cutoff, an abrupt shift (~ 0.6 eV shift to higher binding energy) was observed at the deposition of 0.5 nm In (not shown here). This may also relate to the charge transfer between In and ZnPc, although further studies are needed.

With the increase of the In thickness, the intensity of in-gap state was decreased. In addition, the signal from the HOMO of ZnPc was observed on the spectrum with 20 nm deposition of In. These results indicate that: (i) the distance between the In atom and the ZnPc molecule was an important parameter for the formation of the in-gap state, (ii) In atoms were diffused into the ZnPc layer.

Note that the interface state was not observed in the spectra of ZnPc on the In layer. (Fig. 2) This result indicates that the order of the deposition critically affects the electronic state of the interface. A driving force of the diffusion of In atoms into the ZnPc layer

is probably needed for the formation of the in-gap state.

Based upon these results it is expected that there is a difference in the carrier transfer properties between the In-on-ZnPc interface and the ZnPc-on-In interface. It is known that the rectifying contact is formed at the In-on-ZnPc interface [3]. Investigations of the effects of the interface states on the electric properties of the ZnPc/In interface are now in progress.
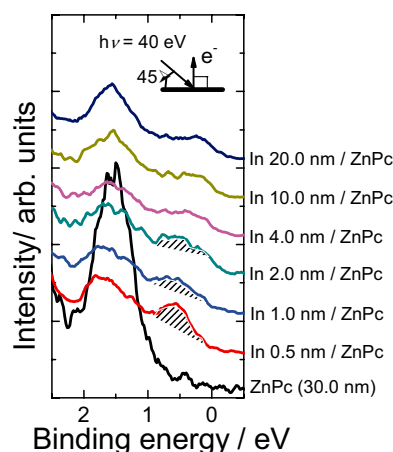
Fig. 1. Photoelectron spectra of In incrementally deposited on the ZnPc layer. An in-gap state (hatched) was observed for the low-thickness region.
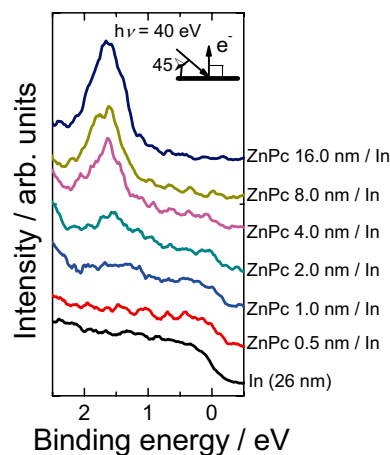
Fig. 2. Photoelectron spectra of ZnPc incrementally deposited on the In layer.

[1] Y. Hirose *et al.*, Phys. Rev. B **54** (1996) 13748.
[2] V. Yu. Aristov *et al.*, Phys. Rev. B **72** (2005) 165318.
[3] M. Nonomura *et al.*, Appl. Phys. Lett. **88** (2006) 042111.

Ⅲ-4. SURFACE AND THIN FILMS